Journal of Nuclear Materials 390–391 (2009) 727–732

Contents lists available at ScienceDirect

Journal of Nuclear Materials

journal homepage: www.elsevier.com/locate/jnucmat

Physics of ELM power fluxes to plasma facing components and implications for ITER

A. Kirk [a,*], S. Lisgo [a], E. Nardon [a], T. Eich [b], A. Herrmann [b], A. Kallenbach [b], A. Loarte [c]

[a] EURATOM/UKAEA Fusion Association, Culham Science Centre, Abingdon, Oxon OX14 3DB, UK
[b] Max-Planck Institut für Plasmaphysik, EURATOM Association, Garching, Germany
[c] ITER Organization, Cadarache, St. Paul-lez-Durance, France

ARTICLE INFO

PACS:
52.35.Py
52.40.Hf
52.55.Fa

ABSTRACT

A comparison of the spatial and temporal evolution of the filamentary structures observed during type-I ELMs is presented from a variety of diagnostics and machines. The filaments are elongated in the perpendicular (poloidal) direction and both the radial and poloidal size appears to increase linearly with the minor radius of the machine. The filaments spend between 50 and 100 μs rotating toroidally/poloidally with velocities close to that of the pedestal. Subsequently their rotation velocity decreases and the filaments propagate radially. At the time of separation each filament contains up to 2.5% of the energy released by the ELM. In both the connected and separated stages the dominant loss mechanism is ion parallel transport. The target e-folding length is observed to be correlated with the radial size of the filaments. This may suggest that the physics that drives the size of the filaments also determines the target power e-folding lengths.

1. Introduction

Extrapolations for the amount of energy released by type-I edge localised modes (ELMs) in ITER, based on data from existing tokamaks, indicate that the largest ELMs could not be tolerated because of the damage they would cause to material surfaces [1]. However, there is considerable uncertainty associated with such predictions because of the lack of understanding of all of the processes involved. If the understanding of at least some aspects of the ELM event can be improved, it would mean that models could be further constrained and a reduction in the uncertainty of the predictions for ITER obtained.

The peeling-ballooning mode theory is now widely accepted as the explanation for the observed pressure gradient limit prior to a type-I ELM [2]. This model predicts that type-I ELMs in tokamaks will onset due to an instability with a toroidal mode number in the range 10–20 [3]. It has been suggested [4,5] that the ELM evolution can be broken down into three distinct phases: (1) the linear growth stage of the mode resulting in localised structures inside the Last Closed Flux Surface (LCFS), (2) the rapid growth and formation of filaments that extend outside the LCFS during which there is a rapid loss of energy from the pedestal and (3) the separation of these filaments from the core and their radial motion towards the first wall/limiters.

There is clear evidence for the first stage (see [6] and references therein) in which localised structures exist inside the LCFS just before the onset of an ELM. From the mode number and size of these structures it seems reasonable to assume that these are the precursors to the filament structures that have been observed in the onset (stage 2) of the ELM in a wide range of tokamaks using a variety of diagnostics (see [6] and references therein). It is in the third stage of this process, when there is a clear gap between the plasma in the filament and the core plasma that energy and particles are transported to the limiters/walls. What is not so clear is what role the filaments play in transporting particles and heat to the target near to the strike point during the second stage of the process. In this paper a comparison of the evolution, radial extent and spatial structure of type-I ELMs on a range of devices will be presented and the effects that the filaments have on transporting energy to the targets will be discussed.

2. The separated phase of the filaments and the transport of energy to the wall

In order to make a quantitative prediction for the amount of power arriving outside the divertor, what is required is information on the size, loss mechanism, energy content and motion of the separated filaments. The separated stage is defined as that period when the distance between the centre of the filament and the LCFS is greater than the radial size of the filament and hence a dip would be observed in the radial density profile between the LCFS and the filament. In this section what is known about each of these quantities will be reviewed.

The size of the filaments has been determined on a range of devices using several different techniques, including: measuring the

* Corresponding author.
E-mail address: andrew.kirk@ukaea.org.uk (A. Kirk).

0022-3115/$ - see front matter
doi:10.1016/j.jnucmat.2009.01.198

temporal widths of peaks observed in ion saturation current measurements, visible and infrared imaging, Thomson Scattering and beam emission spectroscopy (see [6] and references therein). These measurements have determined the size of the filaments in both the radial direction (δ_r) and perpendicular to both the field line and the radial direction ($\delta_\perp$). For a conventional aspect ratio device $\delta_\perp$ is primarily in the poloidal direction. Compilations of the radial widths have been published in [6] and [7] and the perpendicular widths in [6]. On all devices the radial extent is smaller than the perpendicular extent, although it should be noted that the ratio is smaller on MAST than on conventional aspect ratio devices. Fig. 1(a) plots the measured perpendicular size of the filaments ($\delta_\perp$) as a function of minor radius. Note the measurements represent the full width of the distributions. Although there is a large spread in the limited dataset, the data are consistent with an increase in size with increasing machine. A linear fit has been performed to the data and the shaded area represents the $\pm1\sigma$ region, which can be used to predict that filaments on ITER will have perpendicular sizes between 23 and 30 cm. Fig. 1b is a plot of the radial filament size (δ_r) with minor radius. Obtaining a simple scaling with minor radius is not so simple here since the radial extent on MAST is larger than that on AUG and DIII-D but similar to that on JET and JT-60U. However, if the results from MAST (open square) are excluded by arguing that the magnetic geometry is different on a spherical tokamak then it is possible to extract a linear fit to the remaining data, which would indicate that the filaments would have a radial extent of between 7 and 10 cm on ITER.

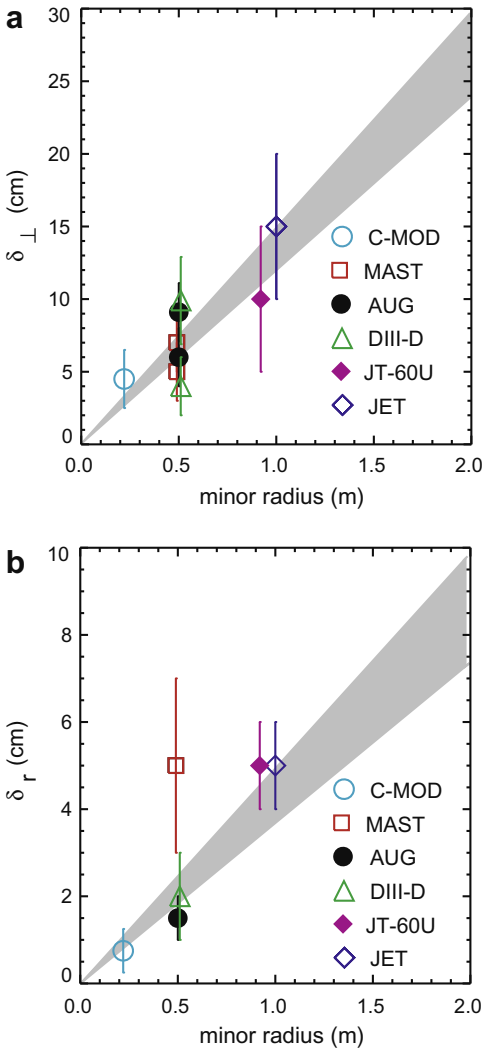

Fig. 1. The (a) perpendicular and (b) radial size of the filaments as a function of machine minor radius. The shaded area represents the $\pm1\sigma$ region of a fit to the data. In (b) the open square (MAST data) has been omitted from the fit.

There is a general consensus [5,7–9] about the loss mechanism for the separated filaments: the electrons cool through parallel transport more rapidly than the ions and the density is removed on ion parallel transport loss times. This is based on a number of observations, including: (1) that the particle content of the filaments decreases exponentially with distance from the LCFS, (2) that the electron temperature in the filament decreases more rapidly [10] than the ion temperature [11,12] and (3) the light front associated with the filaments has been observed to extend along the field line towards the target with a parallel velocity consistent with the ion sound speed [13].

In order to measure the energy content of the filament the density, electron and ion temperatures and the filament volume are required. On MAST and JET the radial density and electron temperature profiles of filaments, obtained from Thomson scattering, have been combined with the measured perpendicular size and the assumption that the filament extends between the top and bottom of the plasma on the low field side to calculate the energy content assuming $T_i = T_e$ [13,14] (although as indicated above $T_i > T_e$ may be a better assumption). The maximum energy content of a single filament, observed close to the LCFS on both devices, is 2.5% of ΔW_{ELM}, this may well be an underestimate of the maximum size since it assumes that $T_i = T_e$. These observations would suggest that the maximum amount of ELM energy transported to the wall would be 25% ($T_i = T_e$) or 50% ($T_i = 3T_e$) for 10 equally sized filaments. Note that this assumes all the filaments have the maximum size observed and hence is likely an over estimate. In order to account for the spread in filament energy content and the uncertainty in the value of T_i, in the remainder of the paper the average filament energy content is assumed to be 2.5% of ΔW_{ELM}.

Finally in order to determine the impact of the filaments on the first wall, information on the parameters affecting the filament propagation is required. A summary of the measurements of the toroidal/poloidal velocities from all devices where data are available is given in Ref. [6]. All the measurements agree that the filaments initially rotate in the co-current direction with velocities near to the pedestal values, which then decrease with time and distance into the scrape off layer (SOL). Where there is more disagreement is in the radial propagation.

The radial propagation of the filaments has been determined by a number of techniques, which have indicated all possibilities for the dependence of the radial velocity of the filament as a function of distance from the LCFS i.e. constant, deceleration and acceleration [6]. Some of these differences arise because of the different techniques used to measure the velocities while others are most likely due to the difficulties of measurement techniques e.g. trying to determine the electric field within a filament or determining the velocity of a filament from time of flight when the start time is not known accurately. As an example, recent measurements from ASDEX Upgrade have used the time difference between the peaks in the I_{SAT} recorded by two Langmuir probes that were separated by 5 mm [15]. Fig. 2(a) shows a plot of the calculated radial velocity, using the time difference between the probes, as a function of distance from the LCFS for the raw data (solid circles) and the mean velocity binned as a function of distance (open circles). The data are consistent with a constant radial velocity of 1.5 kms^{-1} (solid line). Fig. 2b shows radial velocity calculated from the same data using the time difference between the start of the ELM (determined by the rise time of the D_α light) and the peak in the I_{SAT} trace of the first probe. The velocity calculated with this method appears to increase with distance and the mean is much lower (0.2 kms^{-1}). The reason for the discrepancy is due to the fact that the filaments

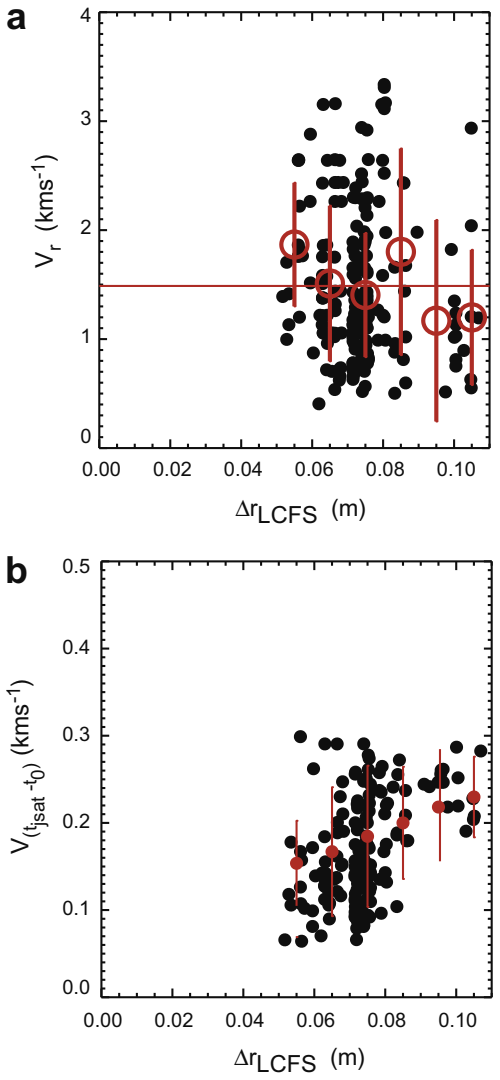

Fig. 2. The radial velocity of ELM filaments on AUG (a) determined from two radially separated probes and (b) determined using the time of flight from the start of the ELM as a function of distance from the LCFS.

do not all leave the LCFS at the same time and they do not begin to separate until 50–200 μs after the start of the rise in the D_α light. Hence, the latter measurement technique is less reliable.

Taking into account the evidence from all devices and techniques it is most likely that the filaments do not slow down substantially when far out into the SOL and before they have interacted with the nearest limiter surface. Typical radial velocities range from 500 to 2 kms^{-1} [6].

3. The connected stage and the effect of the filaments on divertor target profiles

Filaments exist near the LCFS for 50–100 μs at the start of the ELM event and are born as elongated field aligned structures, which have an initial parallel extent covering the low field side of the plasma. The rise time of the divertor ELM energy flux is correlated with the ion transport time [16], and a detailed analysis of the temporal evolution of the ELM power target deposition in AUG and JET reveals that the ELM energy must be released from the core in $\leqslant$80 μs [17]. This ELM energy loss time is similar to that found from a study of the time evolution of the pedestal using the multi-time point Thomson scattering profiles on MAST [13]. These show that effectively the entire loss from the pedestal occurs in less than 200 μs (the time between two profiles). Line integral density measurements, which measure not only the core but also the SOL, decrease on a longer time scale because the SOL density has been increased due to the ELM and it is depleted on ion parallel transit times [13].

The power deposition profile at the targets, both in inter-ELM periods and during ELMs, is often parameterised in terms of a double exponential, with one component describing the sharp fall-off in the near SOL (λ_{near}) combined with a second exponential in the far SOL (λ_{far}) due to the filament motion. The narrow λ_{near} is traditionally thought to be conduction dominated leading to a prediction that the power e-folding length (λ_q) should be related to the temperature e-folding length (λ_{Te}) by $\lambda_q = \frac{2}{7}\lambda_{T_e}$ [18]. Comparison of mid-plane inter-ELM temperature e-folding lengths from a variety of devices was compiled in Ref. [18] where a good scaling with major radius of the device was observed leading to a prediction on ITER for the temperature e-folding length of $\lambda_{T_e}^{ITER} = 18$ mm. This has been used, assuming conduction dominance, to predict the power fall-off length for ITER of $\lambda_{Te}^{ITER} = 5$ mm. The data from MAST was not included in this study. Fig. 3(a) shows a plot of λ_{Te} versus major radius from Ref. [18] to which the data from MAST has been included. The MAST point clearly does not fit the trend observed from the other conventional aspect ratio devices. This is similar to what was observed in the plot of filament size versus minor radius in Fig. 1b. Fig. 3b shows a plot of λ_{Te} versus radial filament size where a clear correlation can be observed. For each device the two values come from discharges with similar plasma parameters but they are not from the same discharge. Also λ_{Te} is determined from inter-ELM data and δ_r is for ELM filaments However, data from AUG [19] and MAST [20] show that filaments also exist in inter-ELM periods and that their radial size is similar to the ELM filaments. Also it is widely observed that the target width is the same inter-ELM and during ELMs [21].

Though there are still many uncertainties in due to the lack of available data one conclusion that could be drawn from this plot is that the physics that determines the filament size also determines λ_{Te}. It is also possible to speculate that filament based radial transport is determining λ_{Te}.

In order to build a model for both the near and far regions knowledge of how the energy is transported to the targets is required. In order to test if electron conduction does dominate the near region the target power e-folding length (λ_q), mapped back to the mid-plane, has been calculated from published data from C-MOD [22], AUG [21], MAST [13] and JET [21] and compared to the measured values of λ_{Te} obtained in each case in a similar discharge and is plotted in Fig. 3c. As can be seen the data do not agree with $\lambda_q = \frac{2}{7}\lambda_{T_e}$. A fit to the data yields $\lambda_q = 0.8\lambda_{T_e}$, i.e., it is more consistent with convection dominance. This is consistent with the observation that the ELM energy arrives at the target on ion transit times [16]. PIC simulations of ELMs [23,24], taking into account electrons and ions, show that the power is mainly carried by the ions (70%) and that both the electrons and the ions deposit most of the power on the ion time scale i.e. there is no evidence of a large conducted component.

4. Modelling the structure of ELM power loads

Based on the observations presented in this paper the most probable ELM energy loss process is as follows: for the first 50–100 μs, filaments remain near to the LCFS. During this time the filaments enhance losses with an e-folding length that is determined by their radial size. This could either be because the filaments compress the flux surfaces at the edge, and hence increase the radial

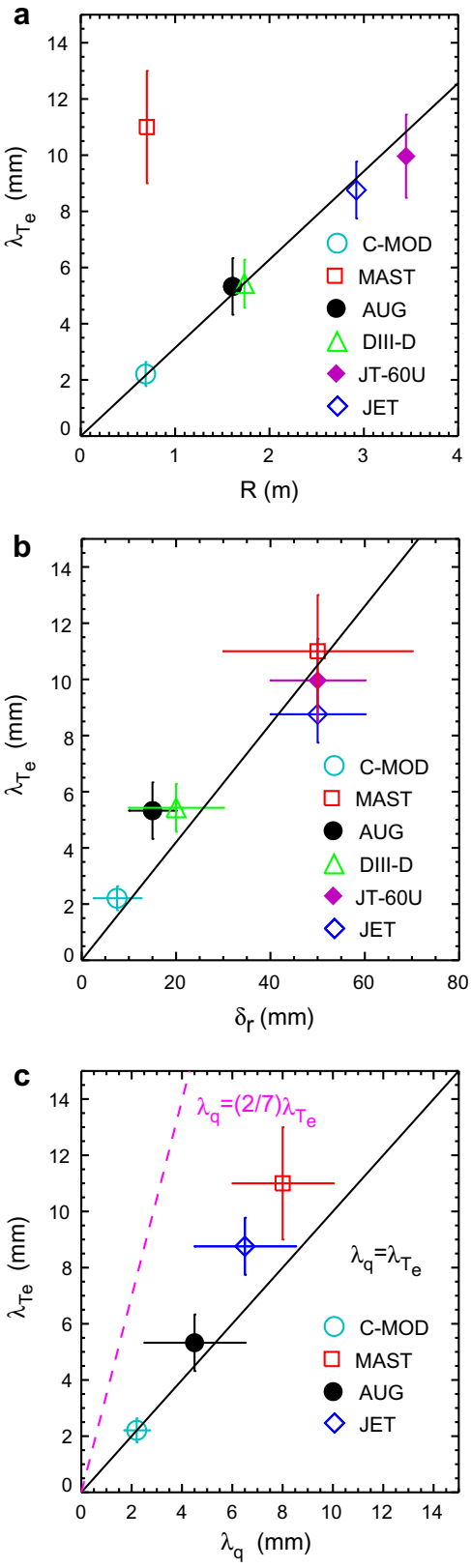

Fig. 3. Mid-plane temperature e-folding (λ_{Te}) length versus (a) machine major radius, (b) radial size of the filament and (c) the power e-folding length.

transport, or that a reconnection occurs of one end of the filament into the SOL near the x-point leading to a direct path from the core plasma. In either case the radial size of the losses would be correlated with the filament size. After this time the filaments move radially away from the LCFS with each filament containing up to 2.5 % of ΔN_{ELM} and ΔW_{ELM} which is subsequently lost by parallel transport along open field lines to the targets. This representation of the ELM event has been incorporated into a Monte Carlo code in order to simulate the target power profiles assuming that the process is dominated by ion parallel transport. The simulation starts by creating a filament in which 1 million particles are distributed according to a Gaussian (with a machine dependent σ as determined from Fig. 1) in the radial and perpendicular directions and uniformly along a distance ±L. Each particle has a velocity as derived from a Maxwellian velocity distribution according to an initial temperature (taken to be half of the pedestal height) and N such filaments are created. There are two stages of the process: (1) the stage during which the filaments are assumed to be connected to the core of the plasma and (2) the stage in which the filaments have separated from the core and travel radially. During the first stage each filament, and hence each particle within the filament, starts off with zero radial velocity and a toroidal velocity compatible with that of the pedestal. At the time of separation the toroidal velocity has been reduced to zero and the radial velocity is increased either to a constant or increasing velocity. At the time of separation it is ensured (by adjusting the number of particles) that the energy content of each filament is 2.5% of the total amount of energy simulated. Each particle within each filament is tracked along the relevant field line until it arrives at either the divertor target or intersects the wall. The number of particles and the mean absolute velocity of each particle are recorded as a function of time and position and are used to represent the density and ion temperature. Such a simulation has previously been able to successfully describe the target profiles and the fraction of power arriving at the targets on MAST [13] and AUG [25] and here it is used to predict the values for ITER. It should be noted that although the simulation predicts the target profile in AUG it would not predict the in-out target load asymmetries observed [17]. To explain the large fraction of ELM energy arriving at the high field side target an additional loss process, for example the fast ion loss mechanism described in [26], would be required.

The simulation for ITER starts off with 12 filaments each parameterised to have a Gaussian profile with $\sigma_r = 1.6$ cm and $\sigma_\perp = 5$ cm, based on the extrapolations obtained from Fig. 1 and by defining the full width obtained as being 5σ. The initial ion temperature in the filament is assumed to be half of the pedestal top, i.e., 1.5 keV. For a period of 50 μs half of the filament protrudes from the LCFS and the filaments rotate with the pedestal velocity and release particles into the SOL. After this time individual filaments decelerate toroidally and move away radially, each carrying up to 2.5% of the total number of particles lost. In both the connected and separated stage the particles are traced along the local field line to the divertor target. As was discussed above, determining the radial velocity of the filaments on current devices is difficult and relies on several assumptions, which makes extrapolations prone to error. To demonstrate the sensitivity of the results to the radial velocity used, two simulations have been performed using values of $V_r = 0.5$ and 1 kms^{-1}. These values are at the extremes of the extrapolations found in [5], which were made using the parallel loss limit of a sheath resistive model.

The resulting mid-plane density and ion temperature profiles are shown in Fig. 4(a) and (b). Typically between 15 and 40% of the initial particle content of the filaments reaches the wall with ion temperatures in the range of 200–500 eV. The profiles have been fitted with an exponential in the region $0.02 < \Delta r_{LCFS} < 0.06$ and yield e-folding lengths of $\lambda_{ne} = 2.8$ (5.6) cm and $\lambda_{Ti} = 3.6$ (5.7) cm for $V_r = 0.5$ kms^{-1} ($V_r = 1$ kms^{-1}). These values are similar to those found using a fluid based model where the parallel losses are treated with diffusive and advective removal times [27].

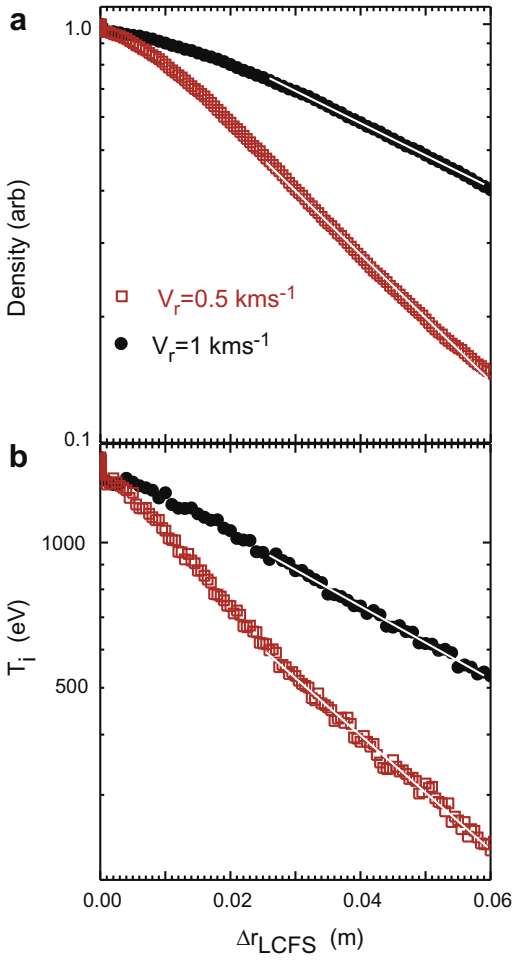

Fig. 4. Results of a simulation for ITER of the mid-plane (a) density and (b) ion temperature profiles as a function of distance from the LCFS for filaments with two radial velocities.

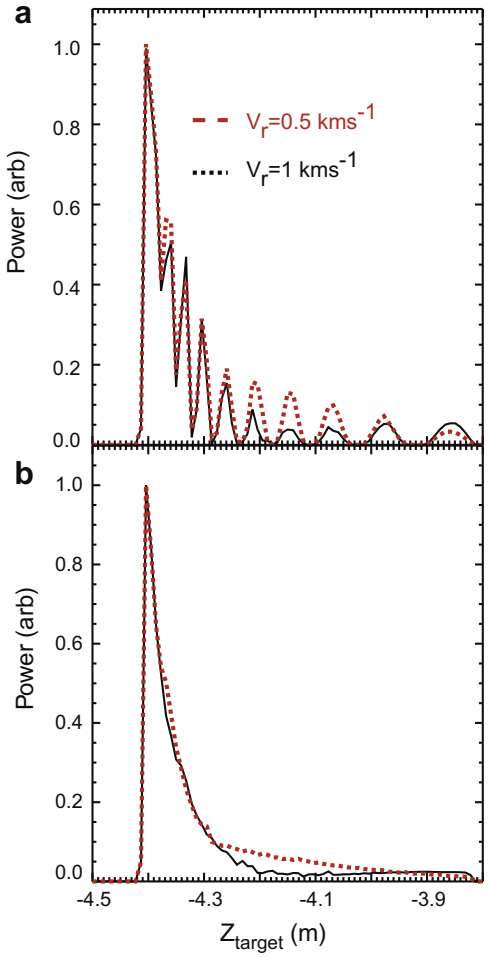

Fig. 5. The predicted target distributions on ITER (a) at a given toroidal location and (b) toroidally averaged for filaments with two radial velocities.

The simulation can also be used to predict the divertor target profile and the fraction of power arriving at the limiter, which is located 6 cm from the LCFS at the mid-plane and in the tail of the target profile. The resulting target profiles at a particular toroidal location are shown in Fig. 5(a) and integrated over all toroidal angles in Fig. 5(b). Significant structure can be observed in the remote region of the target. The target sheath transmission coefficient is assumed to be constant in time; this assumption could affect the ratio of the power at the separatrix to that at the remote regions of the target.

In order to calculate the amount of energy arriving at the limiter a 2D profile of the ITER limiter has been incorporated into the model. If a particle in the filament intercepts with the limiter before arriving at the target its energy is assumed to have been deposited at the limiter. The fraction of the ELM energy deposited on the limiter is 4.0 (15.5)% for $V_r = 0.5$ kms^{-1} ($V_r = 1$ kms^{-1}). The fraction of energy arriving in the tail of the target profile, defined as $Z > -4.2$ m, is 17.7 (10.9)%.

5. Summary

In this paper a summary of the results on the size and motion of filaments observed during type-I ELMs has been presented. The size of the filaments has been studied on a variety of devices and there is evidence that the filaments do not have a circular cross section instead they are elongated in the perpendicular (poloidal) direction. The results from all the tokamaks presented are consistent with the perpendicular size increasing linearly with the minor radius of the machine giving an estimate for their size on ITER as $\delta_\perp = 23$–30 cm. Obtaining a scaling for the radial size is more difficult, but the best estimate for ITER, again assuming this scales with the size of the machine, is $\delta_r = 7$–10 cm. The radial size of the filament is correlated with the mid-plane temperature e-folding length, which suggests that they are both determined by the same physical process. Although, the physics behind this process is not yet known, the fact that there is a difference in the widths between large and small aspect ratio machines will allow future models to be tested.

Turning now to the motion of the filaments, the filaments start off rotating toroidally/poloidally with velocities close to that of the pedestal. This velocity then decreases as the filaments propagate radially. It is most likely that the radial velocity of the filaments does not decrease substantially when far out into the SOL and typical velocities are in the range 0.5–2 kms^{-1}. The rate limiting loss mechanism is through ion parallel transport and the transport to the wall is through the radial propagation of these filaments. Measurements of the filament energy content show that each filament contains up to 2.5% of the energy released by the ELM at the time it separates from the LCFS and it would appear that the dominant energy loss has occurred while the filaments are still attached to the LCFS. This information has been combined in a Monte Carlo simulation, which is able to describe the target profiles on AUG and MAST and to make predictions for ITER.

Acknowledgements

UKAEA authors were funded jointly by the United Kingdom Engineering and Physical Sciences Research Council and by the European Communities under the contract of Association between EURATOM and UKAEA. The views and opinions expressed herein do not necessarily reflect those of the European Commission.

References

[1 A. Loarte et al., Plasma Phys. Control. Fus. 44 (2002) 1815.
[2] J.W. Connor et al., Phys. Plasmas 5 (1998) 2687.
[3] P.B. Snyder et al., Plasma Phys. Control. Fus. 46 (2004) A131.
[4] A. Kirk et al., Phys. Rev. Lett. 92 (2004) 245002.
[5] W. Fundamenski, R.A. Pitts, Plasma Phys. Control. Fus. 48 (2006) 109.
[6] A. Kirk et al., J. Phys.: Conf. Ser. 123 (2008) 012011.
[7] B. Lipshultz et al., Nucl. Fus. 47 (2007) 1189.
[8] A.W. Leonard et al., Plasma Phys. Control. Fus. 48 (2006) A149.
[9] K. Kamiya et al., Plasma Phys. Control. Fus. 49 (2007) S43.
[10] J.A. Boedo et al., Phys. Plasmas 12 (2005) 072516.
[11] R.A. Pitts et al., Nucl. Fus. 46 (2006) 82.
[12] A. Herrmann et al., J. Nucl. Mater. 363–365 (2007) 528.
[13] A. Kirk et al., Plasma Phys. Control. Fus. 49 (2007) 1259.
[14] M. Beurskens et al., Pedestal dynamiscs in ELMy H-mode plasmas in JET, Paper EX/P3-4, in: Proceedings of 22nd IAEA Fusion Energy Conference, Geneva, Switzerland, 2008.
[15] A. Schmid et al., Plasma Phys. Control. Fus. 50 (2008) 045007.
[16] T. Eich et al., J. Nucl. Mater. 337–339 (2005) 669.
[17] T. Eich et al., in: Proceedings of 34th EPS Conference on Plasma Physics and Controlled Fusion P-2.017, 2007.
[18] A. Kallenbach et al., J. Nucl. Mater. 337–339 (2005) 381.
[19] B. Kurzan et al., Plasma Phys. Control. Fus. 49 (2007) 825.
[20] N. Ben Ayed et al., Plasma Phys. Control. Fus. 51 (2009) 035016.
[21] A. Herrmann et al., J. Nucl. Mater. 313–316 (2003) 759.
[22] B. LaBombard et al., Phys. Plasmas 2 (1995) 2242.
[23] A. Bergmann, Nucl. Fus. 42 (2002) 1162.
[24] D. Tskhakaya et al., in: Proceedings of 34th EPS Conference on Plasma Physics and Controlled Fusion O-2.002, 2007.
[25] A. Kirk et al., J. Phys.: Conf. Ser. 123 (2008) 012012.
[26] A. Kallenbach et al., Nucl. Fus. 48 (2008) 085008.
[27] W. Fundamenski, R.A. Pitts, J. Nucl. Mater. 363–365 (2007) 319.